Title

A post-processing method based on interphase motion correction and averaging to improve image quality of 4D magnetic resonance imaging: a clinical feasibility study

Journal

British Journal of Radiology, 92(1095)

ISSN

0007-1285

Authors

Deng, Zixin
Pang, Jianing
Lao, Yi
et al.

Publication Date

2019-03-01

DOI

10.1259/bjr.20180424

Peer reviewed

BJR

https://doi.org/10.1259/bjr.20180424

Received: 10 May 2018 | Revised: 26 October 2018 | Accepted: 11 December 2018

Cite this article as:
Deng Z, Pang J, Lao Y, Bi X, Wang G, Chen Y, et al. A post-processing method based on interphase motion correction and averaging to improve image quality of 4D magnetic resonance imaging: a clinical feasibility study. *Br J Radiol* 2019; **92**: 20180424.

FULL PAPER

A post-processing method based on interphase motion correction and averaging to improve image quality of 4D magnetic resonance imaging: a clinical feasibility study

[1]ZIXIN DENG, PhD, [2]JIANING PANG, PhD, [3]YI LAO, PhD, [4]XIAOMING BI, PhD, [1]GUAN WANG, MD, [1]YUHUA CHEN, MS, [5]MATTHIAS FENCHEL, PhD, [3]RICHARD TULI, MD, [1,6,7]DEBIAO LI, PhD, [1,3]WENSHA YANG, PhD and [1,6,7]ZHAOYANG FAN, PhD

[1]Department of Biomedical Sciences, Biomedical Imaging Research Institute, Cedars Sinai Medical Center, Los Angeles, CA, USA
[2]MR R&D, Siemens Healthineers, Chicago, IL, USA
[3]Department of Radiation Oncology, Cedars Sinai Medical Center, Los Angeles, CA, USA
[4]MR R&D, Siemens Healthineers, Los Angeles, CA, USA
[5]MR R&D, Siemens Healthineers, New York, NY, USA
[6]Department of Bioengineering, University of California, Los Angeles, CA, USA
[7]Department of Medicine, University of California, Los Angeles, CA, USA

Address correspondence to:
Dr Zhaoyang Fan
E-mail: *zhaoyang.fan@cshs.org*
Wensha Yang
E-mail: *wensha.yang@cshs.org*

The authors Wensha Yang and Zhaoyang Fan contributed equally to the work.

Objective: Four-dimensional MRI (4D-MRI) has been increasingly used in radiation therapy. Developments in *k*-space sorted 4D-MRI methods have shown advantage over conventional image sorted 4D-MRI methods. However, this type of technique tends to suffer from undersampling image artifacts. This study aims to conduct an initial clinical feasibility study of a post-processing method, denoted as MoCoAve, to overcome the limitation.

Methods: Nine patients (seven pancreas, one liver, and one lung) were recruited. 4D-MRI was performed using two prototype *k*-space sorted techniques, stack-of-stars (SOS) and koosh-ball (KB) acquisitions. Post-processing using MoCoAve was implemented for both methods. Image quality score, apparent SNR (aSNR), sharpness, motion trajectory and standard deviation (σ_GTV) of the gross tumor volumes were compared between original and MoCoAve image sets.

Results: All subjects successfully underwent 4D-MRI scans and MoCoAve was performed on all data sets. Significantly higher image quality scores (2.64 ± 0.39 *vs* 1.18 ± 0.34, $p = 0.001$) and aSNR (37.6 ± 15.3 *vs* 18.1 ± 5.7, $p = 0.001$) was observed in the MoCoAve images when compared to the original images. High correlation in tumor motion trajectories in the super-oinferior direction (SI: 0.91 ± 0.08) and weaker in the anteroposterior (AP: 0.51 ± 0.44) and mediolateral (ML: 0.37 ± 0.23) directions, similar image sharpness (0.367 ± 0.068 *vs* 0.369 ± 0.072, $p = 0.805$), and minimal average absolute difference (0.47 ± 0.34 mm) of the motion trajectory profiles was found between the two image sets. The σ_GTV in pancreas patients was significantly ($p = 0.039$) lower in MoCoAve images (1.48 ± 1.35 cm^3) than in the original images (2.17 ± 1.31 cm^3).

Conclusion: MoCoAve using interphase motion correction and averaging has shown promise as a post-processing method for improving *k*-space sorted (SOS and KB) 4D-MRI image quality in thoracic and abdominal cancer patients.

Advances in knowledge: The proposed method is an image based post-processing method that could be applied to many *k*-space sorted 4D-MRI methods for improved image quality and signal-to-noise ratio while preserving image sharpness and respiratory motion fidelity. It is a useful technique for the radiotherapy planning community who are interested in using 4D-MRI but aren't satisfied with their current MR image quality.

INTRODUCTION

In radiation therapy treatment planning, accurate estimation of the delivered radiation dose to the tumor while sparing surrounding healthy organs is critical. In the thoracic and abdominal regions, the estimation is complicated by respiratory motion. In current clinical practice, four-dimensional CT (4D-CT) is used as the gold-standard to quantify tumor and organ geometry at different respiratory motion states.[1,2] However, 4D-CT images are prone to stitching artifacts due to the need for resorting on two-dimensional (2D) images. They also suffer from insufficient differentiation of the tumor from surrounding organs due to the lack of soft-tissue contrast.[3] Moreover, 4D-CT exposes patients to ionizing radiation that can be harmful for patients undergoing multiple treatment fractions.

MRI has gained interest in serving as an alternative to 4D-CT due to its superior soft-tissue contrast, flexible imaging orientation, and free of ionizing radiation. Various 4D-MRI techniques such as real-time volumetric acquisitions using fast three-dimensional (3D) sequences[4,5] or multiple 2D acquisitions followed by slice resorting[6–9] have been developed in the past. However, these methods are limited by the achievable spatiotemporal resolution or, in the multiple 2D acquisition cases, suffer from similar stitching artifacts as 4D-CT.

Recent developments in 4D-MRI based on self-gated (or self-navigated) 3D acquisitions and *k*-space data binning have shown great promise in overcoming the above-mentioned limitations.[10–15] However, to achieve a clinically feasible scan time, this type of techniques tends to suffer from undersampling artifacts and low signal-to-noise ratio (SNR) as limited *k*-space information is acquired in certain respiratory phases. The undersampling artifacts become more severe for patients with highly variable breathing patterns as data collected during irregular breathing states may be denoted as outliers and consequently omitted from the final image reconstruction. Advanced image reconstruction methods have been exploited to mitigate undersampling artifacts. However, they are typically acquisition dependent and computationally extensive, thus, making them less ideal for clinical applications. On the other hand, image post-processing methods as a remedy have shown to be relatively independent of the *k*-space acquisition method used and potentially applicable to *k*-space sorted techniques.[14,16–19] This may allow for image quality improvement of 4D-MRI images obtained from various MRI scanners and *k*-space sorted sequences that suffer from undersampling artifacts and low SNR.

One such method is interphase motion correction and averaging in image space, denoted as MoCoAve, that was initially introduced by Buerger et al[14] and recently revisited by Bi et al.[16] Improvement in image quality with this method was seen in some initial feasibility studies in healthy volunteers or anecdotal clinical cases. As such, the usefulness in a clinical setting and a more rigorous assessment of the method in patients with cancerous tumors have not been demonstrated. Here, we conducted a clinical feasibility study of the method on patients with pancreatic, liver, or lung tumors. The effectiveness of MoCoAve was tested on two prototype *k*-space sorted 4D-MRI techniques to show its feasibility in improving overall image quality while preserving the organ structural features and tumor motion.

METHODS AND MATERIALS

Nine patients with previously diagnosed tumors (seven pancreas, one liver, and one lung) were recruited for the study. The study protocol was approved by the institutional review board and written consent was obtained from all subjects before enrollment of the study. 4D-MRI imaging data were acquired on a 3 T clinical scanner (MAGNETOM Verio or Biograph mMR, Siemens Healthcare, Erlangen, Germany) using either of the two prototype sequences, stack-of-stars (SOS) and koosh-ball (KB). Two of the nine patients underwent both SOS and KB 4D-MRI.

Image acquisition

All image acquisitions were performed during free-breathing. In the SOS method, radial sampling with a golden-angle increment is performed within each *k*-space partition.[20] One radial spoke at the same angle is acquired sequentially for all partitions before proceeding to the next golden-angle. The *k*-space center is measured every N_z (the number of partitions) spokes and used to derive the respiratory self-gating signal. In the KB method, spokes are collected using 2D golden means ordering[21] and the self-gating signal is extracted from a superoinferior spoke that is periodically acquired.[10]

Shared imaging parameters were: spoiled gradient recalled echo readout, flip angle = 10°. Specific imaging parameters for SOS were: field of view = 380 × 380 × 206 mm^3, isotropic spatial resolution = $(1.98\ mm)^3$, 104 partitions with 6/8 partial Fourier, 1504 spokes per partition, repetition time/echo time = 4.0/1.6 ms, self-gating signal interval = 312 ms, total acquisition time = 9 min. Specific imaging parameters for KB were: field of view= 400 × 400 × 400 mm^3, isotropic spatial resolution = $(1.56\ mm)^3$, 7,3005 spokes, 256 reconstructed partitions, repetition time/echo time = 5.8/2.6 ms, self-gating signal interval = 98 ms, total acquisition time =~7 min.

Image reconstruction

In SOS, the central three *k*-space samples along each $K_y = K_z = 0$ line were averaged, and the time series of this value were used to generate the respiratory self-gating signal.[15] In KB, the superoinferior spokes periodically acquired were processed with Fourier transform and principle component analysis to extract the respiratory self-gating signal.[10] Acquired imaging data were grouped into 10 respiratory bins according to their breathing amplitude states determined by the self-gating signal. 3D images were then reconstructed from each bin using their respective subset of data. For SOS, each respiratory bin was reconstructed on the scanner using direct gridding. KB images were reconstructed offline using an in-house MATLAB program based on iterative SENSE reconstruction with temporal regularization[22] for joint reconstruction of all bins.

Post-processing with MoCoAve

Following image reconstruction for SOS or KB, MoCoAve was subsequently applied to the reconstructed 10-phase image series

Figure 1. Schematic diagram of the proposed MoCoAve method for 4D-MRI. *k*-space data were sorted into 10 respiratory bins based on the *k*-space self-gating signal and reconstructed into 10 image sets. Motion correction was performed toward a target image (bin1 in this example) prior to averaging of all warped images. Such process was repeated to generate MoCoAve images for all respiratory phases (bin 1–bin 10). 4D-MR, four-dimensional magnetic resonance; KB, koosh-ball; SOS, stack-of-stars.

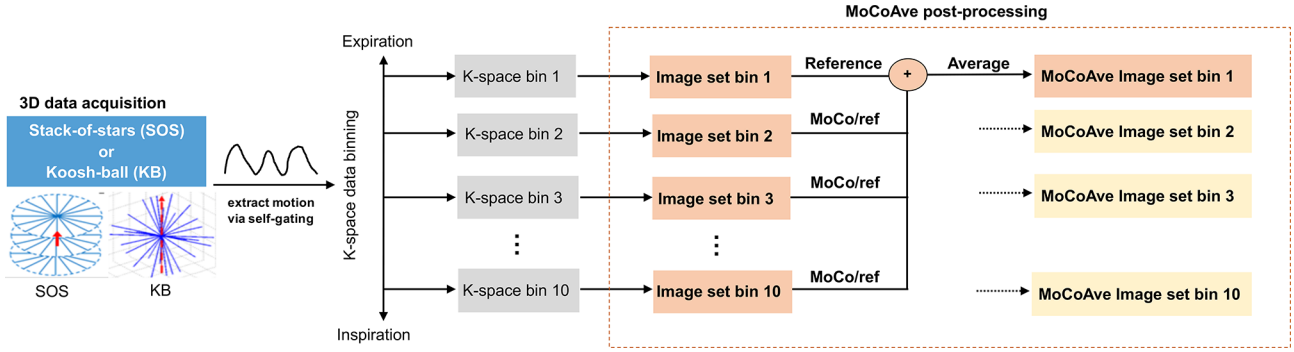

for each patient with an in-house MATLAB program. As shown in Figure 1 under MoCoAve post-processing, forward and inverse transformation between each respiratory phase and a selected reference phase were first calculated using a symmetric diffeomorphic image registration method with a cross-correlation metric.[23] Transformation between two arbitrary phases can then be readily achieved by backward transforming one into the reference phase followed by forward transforming into the selected phase. Following the above procedures, the 3D image set of each specific respiratory phase underwent MoCoAve processing by transforming all other phases to it and averaging them all to achieve a MoCoAve data set for each specific respiratory phase. The overall MoCoAve post-processing took approximately 30 min.

Image analysis

Image sets were randomized and blindly reviewed by two independent reviewers (one medical physicist with 10 year of experience in radiation therapy planning and one radiologist with 5 year of experience in abdominal imaging) using Velocity™ (Varian Medical Systems, Palo Alto, CA). A 3-point scale was used in scoring the image quality: 1, poor (drastic signal loss or severe streaking artifacts and difficult visualization of anatomical structures); 2, fair (minor signal loss or streaking artifacts and adequate visualization of anatomical structures); 3, good (good overall signal intensity, no visible streaking artifacts and good to excellent visualization of anatomical structures). The average scores between the two reviewers were used for the comparison between the original (non-MoCoAve) and MoCoAve image sets.

Apparent SNR (aSNR) was defined as the mean signal intensity in a homogenous region of the liver divided by the standard deviation of the background signal intensity measured in surrounding artifact-free air space. Regions of interest (ROIs) for signal measurement were matched in location and size between non-MoCoAve and MoCoAve image sets.

Image sharpness was measured at three separate locations: (1) interfaces between the tumor and surrounding organ whenever possible or, if the interface was not well defined, at the boundary of a nearby organ in proximity to the tumor; (2) interfaces between the kidney boundary and its surroundings; (3) interfaces between the liver boundary and its surroundings. At each location, three manually drawn boundary-crossing signal intensity profile obtained for sharpness calculation via a previous method,[24] and the mean sharpness among all locations was computed for comparison. All measurement locations were matched between original (non-MoCoAve) and MoCoAve image sets.

The motion trajectory of the tumor in each subject was obtained separately from the non-MoCoAve and MoCoAve image sets. Specifically, gross tumor volumes (GTV) were contoured on the first respiratory phase of the MR images based on the clinical contours from the planning CT images (rigid registration followed by visual assessment and modification). 3D deformable image registration based on the B-spline algorithm was performed across all respiratory bins using Velocity (Varian Medical Systems, Palo Alto, CA). The GTV contours were then mapped to other respiratory bins. The coordinates at the geometric center of each tumor contour were extracted for each respiratory bin and used to determine the motion trajectories. Absolute amplitude difference was calculated between the non-MoCoAve and MoCoAve images based on their respective motion trajectories. In addition, considering pancreatic ductal adenocarcinoma is a firm mass,[25] pancreatic tumor volume is expected to remain constant during breathing. The standard deviation (σ_GTV) of the GTVs for the pancreas subgroup was calculated from all respiratory phases for each 4D-MRI image set, and used as a metric to evaluate GTV consistency during breathing.

Statistical analysis

Wilcoxon signed-rank test was used to determine the differences in image aSNR, image sharpness, image quality scores, and σ_GTV between the non-MoCoAve and MoCoAve approaches using GraphPad Prism software (GraphPad Software Inc., La Jolla, CA). Cross-correlation was used to determine the agreement in the motion trajectory between the two approaches using Microsoft Excel (Microsoft® Excel, Redmond, Washington, WA). In all tests, statistical significance was defined at $p < 0.05$ and data were presented as means ± standard deviations.

Figure 2. Example images comparing MoCoAve and non-MoCoAve images from stack-of-stars (A) and koosh-ball (B) acquisitions. Red circles represent the tumor region. Yellow arrows point at the areas with streaking artifacts in the non-MoCoAve images which is well suppressed in the MoCoAve images.

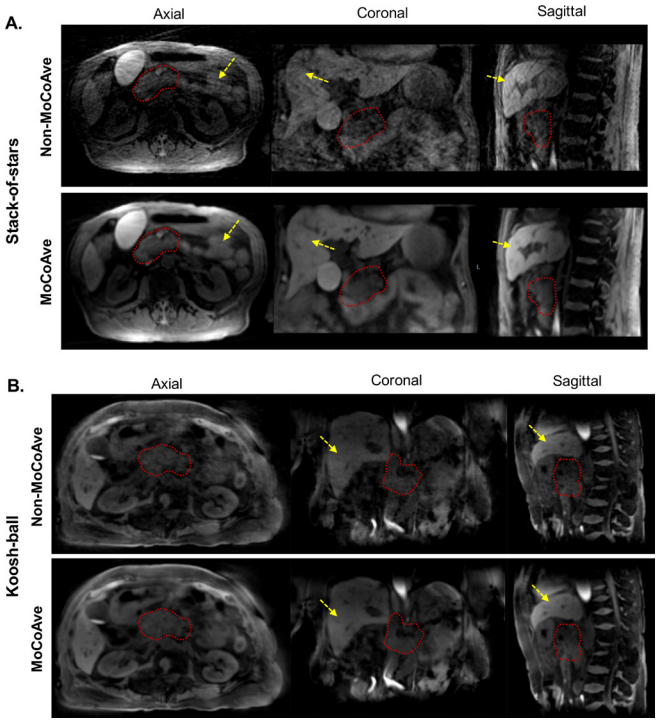

RESULTS

All subjects successfully underwent 4D-MRI scans. Figure 2 shows example images of non-MoCoAve and MoCoAve for both SOS (A) and KB (B) 4D-MRI. In general, the use of MoCoAve remarkably improved aSNR, reduced the image artifacts, and preserved the anatomical details within the organs for both acquisitions. Figures 3 and 4 show MoCoAve SOS and MoCoAve KB image sets, respectively, at end of inspiration, mid-ventilation, and end of expiration.

Figure 3. Example of stack-of-stars acquisition with MoCoAve in end-of-inspiration, mid-ventilation, and end-of-expiration.

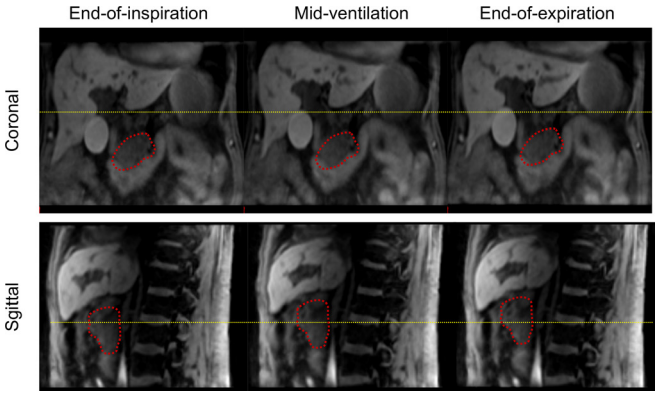

Figure 4. Example of koosh-ball acquisition with MoCoAve in end-of-inspiration, mid-ventilation, and end-of-expiration.

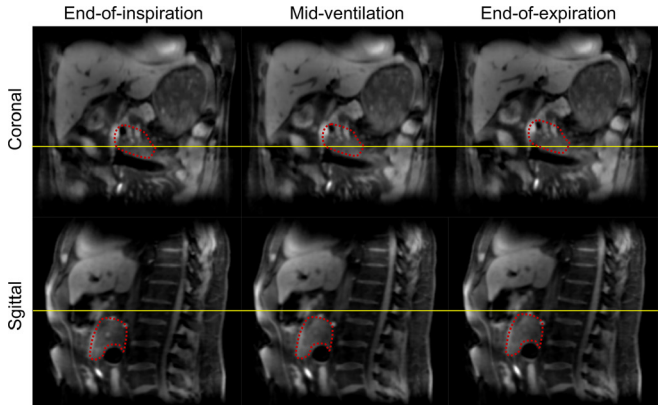

Table 1 summarizes the quantitative analyses of all patients. MoCoAve images showed significantly higher aSNR (37.6 ± 15.3 *vs* 18.1 ± 5.7, $p = 0.001$) and higher image quality scores (2.64 ± 0.39 *vs* 1.18 ± 0.34, $p = 0.001$) when compared to non-MoCoAve images. Strong correlation in tumor motion trajectories between MoCoAve and non-MoCoAve was observed in the superoinferior direction (SI: 0.91 ± 0.08) and weaker in the anteroposterior (AP: 0.51 ± 0.44) and medolateral (ML: 0.37 ± 0.23) directions. Small average absolute difference in the SI direction between the MoCoAve and non-MoCoAve motion trajectories profiles was observed, 0.47 ± 0.34 mm. In addition, similar image sharpness with no significant differences (0.367 ± 0.068 *vs* 0.369 ± 0.072, $p = 0.805$) was also seen when MoCoAve was applied. The σ _GTV in pancreas patients was significantly ($p = 0.039$) lower in MoCoAve images (1.48 ± 1.35 cm^3) than in non-MoCoAve images (2.17 ± 1.31 cm^3).

DISCUSSION

4D-MRI based on self-gated 3D acquisitions and *k*-space data binning[10–15,26] has shown improved image quality and spatial resolution compared with 2D-based 4D-MRI methods,[4–9] resulting in intensified research interest for radiotherapy planning. To further increase its clinical utility, scanning needs to be completed in several minutes, which leads to limited data collection and a highly undersampled *k*-space. This may result in streaking artifacts and low SNR in the reconstructed images. Despite the use of advanced image reconstruction methods, image quality may remain unsatisfactory particularly for patients with irregular breathing patterns that forces larger exclusion of *k*-space data. This work implemented a post-processing method, denoted as MoCoAve, and assessed its clinical feasibility on two prototype *k*-space sorted 4D-MRI techniques, SOS and KB acquisitions. Improved SNR and overall image quality using MoCoAve was demonstrated in patients with pancreatic, liver, or lung tumors.

As a post-processing method, MoCoAve has three advantages for 4D-MRI. First, this is an acquisition independent technique and potentially effective for various *k*-space data binning-based 4D-MRI sequences. In this study, two types of radial sampling sequences were used for MoCoAve processing. Improvement

Table 1. Patient image quality score and correlation coefficient of respiratory motion trajectory between MoCoAve and non-MoCoAve image sets

No.	Age (y)	Sex	Tumor location	Image acquisition type	MocoAve/ non-MocoAve				Motion trajectory			
					aSNR	Image score	Sharpness	σ_GTV	Absolute difference (SI, mm)	Correlation coefficient		
										SI	AP	ML
1	72	M	Lung	SOS	28.3/13.9	3/1.5	0.42/0.40	–	1.18	0.83	–0.36	0.68
2	74	M	Liver	SOS‡	37.8/15.2	3/1	0.36/0.37	–	0.39	0.75	0.70	0.35
3	53	M	Pancreas	SOS	61.8/22.5	2.5/1	0.28/0.26	4.41/4.49	0.36	0.93	0.48	0.65
4	79	M	Pancreas	SOS†	10.9/5.0	2.5/1	0.41/0.42	1.72/2.78	0.49	0.95	0.79	0.45
5	69	M	Pancreas	SOS	49.6/21.1	3/2	0.34/0.34	1.84/2.66	0.37	0.92	0.86	0.32
6	79	M	Pancreas	KB†	19.5/16.8	2/1	0.39/0.40	1.72/1.54	0.06	0.97	0.93	0.44
7	74	M	Liver	KB‡	25.9/17.3	2/1	0.28/0.30	–	0.15	0.78	0.69	0.24
8	79	M	Pancreas	KB	51.8/34.0	2.5/1.5	0.42/0.45	0.95/1.87	0.54	0.95	–0.21	0.20
9	79	F	Pancreas	KB	36.1/19/1	3/1	0.35/0.36	0.34/1.07	0.12	0.96	0.49	0.15
10	35	M	Pancreas	KB	45.0/18.16	3/1	0.36/0.35	0.72/2.73	0.66	0.99	0.32	0.66
11	72	F	Pancreas	KB	46.6/26.1	2.5/1	0.43/0.42	0.14/0.20	0.88	0.96	0.93	–0.04
Mean (STD)	68 (15)				37.6/18.1 (15.3)/(5.7)	2.64/1.18 (0.39)/(0.34)	0.367/0.369 (0.068)/(0.072)	1.48/2.17 (1.35)/(1.31)	0.47 (0.34)	0.91 (0.08)	0.51 (0.44)	0.37 (0.23)
p-value					0.001	0.001	0.805	0.039				

AP, anteroposterior; σ_GTV, standard deviation of gross tumor volume; ML, mediolateral; MoCoAve, motion correction averaging; SD, standard deviation; SI, superoinferior; aSNR, apparent signal-to-noise ratio.

† and ‡ represents the same patient with its respectiveacquisition types.

in image quality appeared independent of acquisition methods. Using a similar approach, Buerger et al also demonstrated such benefits in a Cartesian sampling sequence (golden-radial phase encoding).[13] It is reasonable to anticipate that other acquisition methods could also benefit from the MoCoAve method to improve image quality.[12,27] A standalone image processing package based on the MoCoAve method would be highly desirable to perform more rigorous validations of different 4D-MRI techniques in a clinical setting. Second, the MoCoAve method is especially beneficial for MR acquisition in a relatively random pattern undergoing retrospective *k*-space sorting. In these cases, although reconstructed images may consist of streaking artifacts in one phase, these artifacts are typically distributed in a random fashion among all respiratory phases. By performing interphase motion correction and averaging, the random noise could then be suppressed. This, however, cannot be exploited by other post-processing methods that focused on one image set only. For example, a recently introduced denoising-based method processes each respiratory phase individually, which can result in enhancement of the streaking artifacts as the algorithm may not be able to differentiate between true anatomic structure and patterned artifacts.[17] Third, MoCoAve serves as a remedy to ensure the success of 4D-MRI. The ability can be particularly appreciated in SOS 4D-MRI whereby no advanced image reconstruction had been employed and MoCoAve had significantly improved image quality. This ability is also useful when a scan has to be shortened or is terminated early due to, *e.g.* patient intolerance. Using MoCoAve, acceptable images can be obtained with a reduction of 50% in data for KB 4D-MRI[28] and >80% for the golden-radial phase encoding technique.[14] Clearly, the extent to which *k*-space can be undersampled is application-dependent and warrants more focused investigation.

The risk of image blurring associated with MoCoAve appears to be minimal for the tested imaging protocols. For both acquisitions, MoCoAve and non-MoCoAve showed similar image sharpness and preserved respiratory motion. This suggests that, with our current imaging protocols, the symmetric diffeomorphic image registration method[23] implemented in this work was sufficient to correct for respiratory motion in the abdomen between all respiratory bins. However, it is expected that the performance weakens as original image quality further deteriorates and that more substantial image blurring could happen when applying MoCoAve.

It is interesting to note that, in this study, the consistency in tumor volume (σ_GTV) among 10 respiratory phases in the pancreas subgroup patients was more appreciable in MoCoAve images compared to non-MoCoAve images. The smaller σ_GTV with MoCoAve processing can be attributed to imaging noise.[17] With reduced noise from the MoCoAve 4D-MRI, the B-spline based deformable registration algorithm implemented in Velocity was able to map the tumor boundary to other respiratory bins more consistently. Additionally, previous studies have shown that malignant pancreatic tumors are relatively uncompressible and thus their volumes are likely to remain constant throughout respiratory phases.[25] The lower σ_GTV from the MoCoAve method may in some way represent this phenomenon. However, a larger cohort of patients needs to be studied to better understand the clinical relevance of less tumor volume variation.

This study had some limitations. First, the performance of the MoCoAve method may be dependent on the original quality of the images which is further dependent of the amount of *k*-space data available for reconstruction. In of severe image artifacts, the MoCoAve method may not be able to gain back the clear definition of the anatomical structures. Future sensitivity studies will be needed to determine the limit of MoCoAve to handle these more severely undersampled images. Second, the current study was limited to two radial trajectory sequences. Clinical performance of the proposed method on other sampling trajectories such as Cartesian or spiral trajectories needs to be elucidated on cancer patients.

CONCLUSIONS

The MoCoAve post-processing method using interphase motion correction and averaging has shown promise in improving *k*-space sorted (SOS and KB) 4D-MRI image quality in pancreatic, liver, and lung cancer patients. Significant increases in SNR and image quality can be achieved while image sharpness (tumor and its surrounding organ boundaries) and respiratory motion fidelity are well-preserved. Further rigorous validation in a large-scale clinical study is warranted to establish its applicability for 4D-MRI.

CONFLICT OF INTEREST

Jianing Pang, Xiaoming Bi, Matthias Fenchel are employed by Siemens Healthineers. All other authors have nothing to disclose.

FUNDING

This study was supported by National Institute of Health, National Cancer Institute Small Research Grants (R03) - (Grant No. R03 CA173273).

REFERENCES

1. Keall P. 4-dimensional computed tomography imaging and treatment planning. *Semin Radiat Oncol* 2004; **14**: 81–90. doi: https://doi.org/10.1053/j.semradonc.2003.10.006
2. Rietzel E, Chen GTY, Choi NC, Willet CG, et al. Four-dimensional image-based treatment planning: Target volume segmentation and dose calculation in the presence of respiratory motion. *Int J Radiat Oncol Biol Phys* 2005; **61**: 1535–50. doi: https://doi.org/10.1016/j.ijrobp.2004.11.037
3. Watkins WT, Li R, Lewis J, Park JC, Sandhu A, Jiang SB, et al. Patient-specific motion artifacts in 4DCT. *Med Phys* 2010; **37**(6Part1): 2855–61. doi: https://doi.org/10.1118/1.3432615
4. Dinkel J, Hintze C, Tetzlaff R, Huber PE, Herfarth K, Debus J, et al. 4D-MRI analysis of lung tumor motion in patients with hemidiaphragmatic paralysis. *Radiother*

Oncol 2009; **91**: 449–54. doi: https://doi.org/10.1016/j.radonc.2009.03.021
5. Blackall JM, Ahmad S, Miquel ME, McClelland JR, Landau DB, Hawkes DJ. MRI-based measurements of respiratory motion variability and assessment of imaging strategies for radiotherapy planning. *Phys Med Biol* 2006; **51**: 4147–69. doi: https://doi.org/10.1088/0031-9155/51/17/003
6. Hu Y, Caruthers SD, Low DA, Parikh PJ, Mutic S. Respiratory Amplitude Guided 4-Dimensional Magnetic Resonance Imaging. *Int J Radiat Oncol Biol Phys* 2013; **86**: 198–204. doi: https://doi.org/10.1016/j.ijrobp.2012.12.014
7. Cai J, Chang Z, Wang Z, Paul Segars W, Yin F-F, et al. Four-dimensional magnetic resonance imaging (4D-MRI) using image-based respiratory surrogate: A feasibility study. *Medical Physics* 2011; **38**: 6384–94. doi: https://doi.org/10.1118/1.3658737
8. von Siebenthal M, Székely G, Gamper U, Boesiger P, Lomax A, Cattin P. 4D MR imaging of respiratory organ motion and its variability. *Phys Med Biol* 2007; **52**: 1547–64. doi: https://doi.org/10.1088/0031-9155/52/6/001
9. Tryggestad E, Flammang A, Han-Oh S, Hales R, Herman J, McNutt T, et al. Respiration-based sorting of dynamic MRI to derive representative 4D-MRI for radiotherapy planning. *Med Phys* 2013; **40**: 051909. doi: https://doi.org/10.1118/1.4800808
10. Deng Z, Pang J, Yang W, Yue Y, Sharif B, Tuli R, et al. Four-dimensional MRI using three-dimensional radial sampling with respiratory self-gating to characterize temporal phase-resolved respiratory motion in the abdomen. *Mag Res in Med* 2016; **75**: 1574–85. doi: https://doi.org/10.1002/mrm.25753
11. Rank CM, Heußer T, Buzan MT, Wetscherek A, Freitag MT, Dinkel J, et al. 4D respiratory motion-compensated image reconstruction of free-breathing radial MR data with very high undersampling. *Magn Reson Med* 2017; **77**: 1170–83. doi: https://doi.org/10.1002/mrm.26206
12. Han F, Zhou Z, Cao M, Yang Y, Sheng K, Hu P. Respiratory motion-resolved, self-gated 4D-MRI using rotating cartesian k-space (ROCK. *Med Phys* 2017; **44**: 1359–68. doi: https://doi.org/10.1002/mp.12139
13. Buerger C, Clough RE, King AP, Schaeffter T, Prieto C. Nonrigid motion modeling of the liver from 3-D undersampled self-gated golden-radial phase encoded MRI. *IEEE Trans Med Imaging* 2012; **31**: 805–15. doi: https://doi.org/10.1109/TMI.2011.2181997
14. Buerger C, Prieto C, Schaeffter T. Highly efficient 3D motion-compensated abdomen MRI from undersampled golden-RPE acquisitions. *Mag Res Mat in Phy, Biol Med* 2013; **26**: 419–29. doi: https://doi.org/10.1007/s10334-013-0370-y
15. Grimm R, Fürst S, Dregely I, et al. Self-gated radial MRI for respiratory motion compensation on hybrid PET/MR systems. *Med Image Comput Comput Assist Interv* 2013; **16**: 17–24.
16. Bi X, Pang J, Yang W. Improving Respiratory Phase-resolved 3D Body Imaging Using Iterative Motion Correction and Average (MoCoAve). *International Society of Magnetic Resonance in Medicine Conference, Scientific Session: Abdominal Technique & Pulse Sequences: Oral Presentation* 2016; **24**: 1–3.
17. Jin J, McKenzie E, Fan Z, Tuli R, Deng Z, Pang J, et al. Nonlocal means denoising of self-gated and k-space sorted 4-dimensional magnetic resonance imaging using block-matching and 3-dimensional filtering: implications for pancreatic tumor registration and segmentation. *Int J Rad Onc *Biol* Phy* 2016; **95**: 1058–66. doi: https://doi.org/10.1016/j.ijrobp.2016.02.006
18. Manjón JV, Coupé P, Buades A, Analysis MI. MRI noise estimation and denoising using non-local PCA. *Med Image Anal* 2015; **22**: 35–47. doi: https://doi.org/10.1016/j.media.2015.01.004
19. Sheng K, Gou S, Wu J, Qi SX. Denoised and texture enhanced MVCT to improve soft tissue conspicuity. *Med Phy* 2014; **41**: 101916. doi: https://doi.org/10.1118/1.4894714
20. Winkelmann S, Schaeffter T, Koehler T, Eggers H, Doessel O. An optimal radial profile order based on the Golden Ratio for time-resolved MRI. *IEEE Trans Med Imaging* 2007; **26**: 68–76. doi: https://doi.org/10.1109/TMI.2006.885337
21. Chan RW, Ramsay EA, Cunningham CH, Plewes DB. Temporal stability of adaptive 3D radial MRI using multidimensional golden means. *Magn Reson Med* 2009; **61**: 354–63. doi: https://doi.org/10.1002/mrm.21837
22. Kim D, Dyvorne HA, Otazo R, Feng L, Sodickson DK, Lee VS. Accelerated phase-contrast cine MRI using k-t SPARSE-SENSE. *Magn Reson Med* 2012; **67**: 1054–64. doi: https://doi.org/10.1002/mrm.23088
23. Avants BB, Epstein CL, Grossman M, Gee JC. Symmetric diffeomorphic image registration with cross-correlation: evaluating automated labeling of elderly and neurodegenerative brain. *Med Image Anal* 2008; **12**: 26–41. doi: https://doi.org/10.1016/j.media.2007.06.004
24. Li D, Carr JC, Shea SM, Zheng J, Deshpande VS, Wielopolski PA, et al. Coronary arteries: magnetization-prepared contrast-enhanced three-dimensional volume-targeted breath-hold MR angiography. *Radiology* 2001; **219**: 270–7. doi: https://doi.org/10.1148/radiology.219.1.r01ap37270
25. Crosara S, D'Onofrio M, De Robertis R. Acoustic Radiation Force Impulse (ARFI) of the pancreas. *ESR* 2014;: 1–12.
26. Prieto C, Uribe S, Razavi R, Atkinson D, Schaeffter T. 3D undersampled golden-radial phase encoding for DCE-MRA using inherently regularized iterative SENSE. *Magnetic Resonance in Medicine* 2010; **25**: n/a. doi: https://doi.org/10.1002/mrm.22446
27. Küstner T, Würslin C, Schwartz M, Martirosian P, Gatidis S, Brendle C, et al. Self-navigated 4D cartesian imaging of periodic motion in the body trunk using partial k-space compressed sensing. *Magn Reson Med* 2017; **78**: 632–44. doi: https://doi.org/10.1002/mrm.26406
28. Deng Z, Yang W, Pang J, Bi X, Tuli R, Li D, et al. Improved vessel-tissue contrast and image quality in 3D radial sampling-based 4D-MRI. *J Appl Clin Med Phys* 2017; **18**: 250–7. doi: https://doi.org/10.1002/acm2.12194